Blind Authentication Using Periodic Properties of Interpolation

Babak Mahdian and Stanislav Saic

***Abstract*—In this paper, we analyze and analytically describe the specific statistical changes brought into the covariance structure of signal by the interpolation process. We show that interpolated signals and their derivatives contain specific detectable periodic properties. Based on this, we propose a blind, efficient, and automatic method capable of finding traces of resampling and interpolation. The proposed method can be very useful in many areas, especially in image security and authentication. For instance, when two or more images are spliced together, to create high quality and consistent image forgeries, almost always geometric transformations, such as scaling, rotation, or skewing are needed. These procedures are typically based on a resampling and interpolation step. By having a method capable of detecting the traces of resampling, we can significantly reduce the successful usage of such forgeries. Among other points, the presented method is also very useful in estimation of the geometric transformations factors.**

***Index Terms*—Digital forgery, image forensics, interpolation, interpolation detection, resampling, resampling detection, tampering detection.**

I. Introduction

DESPITE its importance, massive usage[1] and history[2] of interpolation, to our knowledge, there are only a few published works concerned with the specific and detectable statistical changes brought into the signal by this process. In this paper, we analytically describe specific periodic properties present in the covariance structure of interpolated signals and their nth derivatives. Without the detailed knowledge of how the statistics of the signal are changed by the interpolation process, applications based on statistical approaches working with resampled/interpolated signals or with their derivatives can yield miscalculations and unexpected results.

Furthermore, we propose a blind, efficient, and automatic method capable of detecting the traces of resampling and interpolation. The method is based on a derivative operator and radon transformation. The knowledge of whether the given signal or some of its portions has been resampled can play an essential role in many fields, especially in image security and authentication. Without a doubt, image security and authentication are significant in many social areas and play a crucial role in people's lives. For instance, the trustworthiness of photographs has an essential role in courtrooms, where they are used as evidence. Everyday, newspapers and magazines depend on digital images. Today, we face the problem of digital image forgeries even in scientific literature. As a consequence, it is obvious that we should pay special attention to the field of image authenticity. Therefore, we believe in the wide and possible use of the proposed method. Furthermore, the presented method is very useful in estimating the geometric transformations factors as well.

When two or more images are spliced together (for example, see Fig. 1), to create high-quality and consistent image forgeries, almost always geometric transformations, such as scaling, rotation, or skewing, are needed. Geometric transformations typically require a resampling and interpolation step. Therefore, by having sophisticated resampling/interpolation detectors, altered images containing resampled portions can be easily identified and their successful usage significantly reduced.

Existing digital forgery detection methods are divided into active [2]–[4] and passive (blind) [5]–[10] approaches. The passive (blind) approach is regarded as the new direction. In contrast to active approaches, passive approaches do not need any explicit prior information about the image. They work in the absence of any digital watermark or signature. Passive approaches have not yet been thoroughly researched. Different methods for identifying each type of forgery must be developed. Then by fusing the results from each analysis, a decisive conclusion may be drawn.

The rest of this paper is organized as follows. The next section summarizes previous published papers concerned with the topic of this paper. After this, some basic notations and definitions are given to build up the necessary mathematical background. Section IV analyzes and analytically shows hidden periodic properties present in interpolated signals and in their derivatives. In Section V, we study periodic properties brought into the signal by concrete interpolation kernels. Section VI proposes a method capable of detecting the traces of affine transformation. The following section contains experiments which demonstrate the outcomes of the proposed method. In Section VIII, the main properties of the method and its results are discussed. The last section summarizes the work that has been done in this paper.

II. Related Work

In [11], A. C. Gallagher, in an effort to detect interpolation in digitally zoomed images, has found that linear and cubic interpolated signals introduce periodicity in variance function of

Manuscript received July 19, 2007; revised February 25, 2008. First published June 13, 2008; last published August 13, 2008 (projected). This work was supported in part by the Czech Science Foundation under Project no. GACR 102/08/0470. The associate editor coordinating the review of this manuscript and approving it for publication was Prof. Mohan Kankanhalli.

The authors are with the Institute of Information Theory and Automation, Academy of Sciences of the Czech Republic, Prague 8 18208, Czech Republic (e-mail: mahdian@utia.cas.cz; ssaic@utia.cas.cz).

Digital Object Identifier 10.1109/TIFS.2004.924603

[1]For instance, almost every image resizing or rotation operation requires an interpolation process (nearest neighbor, linear, cubic, etc.).

[2]Interpolation has a long history and probably started being used as early as 2000 BC by ancient Babylonian mathematicians. For instance, it had an important role in astronomy which in those days was all about time keeping and making predictions concerning astronomical events [1].

Fig. 1. Example of image forgery based on resampling and interpolation. Shown from left to right are: source image A, source image B, and tampered image. The tampered image has been created by splicing source image A with a resized part of source image B. This part has been resized by scaling factor 1.42 using the bicubic interpolation.

their second-order derivative. This periodicity is simply investigated by computing the discrete Fourier transform (DFT) of an averaged signal obtained from the second derivative of the investigated signal. Furthermore, based on the fact that the mentioned periodicity is directly related to the resampling rate, the author easily estimates the resampling rate. The major weakness of the method is that it cannot be applied to rotated or skewed images.

Another work concerned with the detection of resampling and interpolation has been proposed by S. Prasad and K. R. Ramakrishnan [10]. Similar to [11], the authors have noticed that the second derivative of an interpolated signal produces detectable periodic properties. The periodicity is simply detected in the frequency domain by analyzing a binary signal obtained by zero crossings of the second derivative of the interpolated signal. The major weaknesses of this method are similar to [11].

In an interesting work [7], A. C. Popescu and H. Farid have analyzed the imperceptible specific correlations brought into the resampled signal by the interpolation step. Their method is based on the fact that in a resampled signal, it is possible to find a set of periodic samples that are correlated in the same way as their neighbors. The core of the method is an expectation/maximization (EM) algorithm. The main output of the method is a probability map containing periodic patterns if the investigated signal has been resampled.

As it is apparent, the subject of this paper has not been studied in detail. In this work, we study and analytically describe the periodic properties of the covariance structure of interpolated signals and their derivatives. Using the theory, we bring the main contribution of this paper which is a fast, blind, and efficient method capable of detecting traces of arbitrary affine transformation. The method can be also used for estimating the scaling factors or rotation angles as well as skewing factors. The core of our method is a radon transformation applied to the derivative of the investigated signal. In this paper, among other points, we extend and generalize the theory introduced in [11]. We show that the specific periodicity is present in interpolated signals as well as in their derivatives. We briefly extend the theory for 2-D cases as well. Also, we analyze and show periodic patterns of interpolation by an application of Taylor series to the interpolated signals. To summarize, the main novelties of the paper are the following: the use of the radon transformation making possible the detection of rotation and skewing, the generalization of the theory introduced in [11], and an application of Taylor series to the interpolated signals showing a hidden periodicity.

Obtained results of the proposed method show that it is possible in a simple and fast way to find traces of general affine transformation when a low-order interpolation polynomial has been used. To our knowledge, the only published method comparable with our method is [7]. In comparison to this work, our method works on a much easier principle and is more convenient and faster to implement and run. Another advantage of the proposed method compared to [7] is that it does not need any initialization parameters which can strongly affect obtained outcomes.

III. Basic Notations and Preliminaries

First, a proper mathematical model simulating the acquisition system is required. Periodic properties of interpolation can be effectively studied by using the following simple, linear, and stochastic model and assumptions:

$$f(x) = (u * h)(x) + n(x) \tag{1}$$

where f, u, h, $*$, and n are the measured image, original image, system point-spread function (PSF), convolution operator, and random variable representing the influence of noise sources statistically independent from the signal part of the image. We assume that $E\{n(x)\} = 0$. If we consider the first part of (1) to be deterministic, the covariance of (1) can be shown to be $R_f(x_1, x_2) = Cov\{f(x_1), f(x_2)\} = E\{(f(x_1) - \overline{f}(x_1))(f(x_2) - \overline{f}(x_2))\} = Cov\{n(x_1), n(x_2)\} = R_n(x_1, x_2)$, where R_f is the covariance matrix of measured image $f(x)$, and R_n is the covariance of random process $n(x)$.

We will denote f_k as a discrete signal representing the samples of $f(x)$ at the locations $k\Delta_x$, $f_k = f(k\Delta_x)$, where $\Delta_x \in \mathcal{R}^+$ is the sampling step and $k \in \mathcal{N}_0$.

For the sake of simplicity, we introduce the operator $\mathcal{D}^n\{\bullet\}$, $n \in \mathcal{N}_0$, which is defined in the following way: $\mathcal{D}^n\{f\}(x) = f(x)$ for $n = 0$ and $\mathcal{D}^n\{f\}(x) = \partial^n f(x)/\partial x^n$ for $n \in \mathcal{N}$. In other words, $\mathcal{D}^0\{f\}(x)$ is identical to $f(x)$ and $\mathcal{D}^n\{f\}(x)$, where $n > 0$ is the nth derivative of $f(x)$. In discrete signals,

the derivative is typically approximated by computing the finite difference between adjacent samples.

IV. Hidden Periodicity of Interpolated Signals

There are two basic steps in geometric transformations. In the first step, a spatial transformation of the physical rearrangement of pixels in the image is performed. Coordinate transformation is described by a transformation function T, which maps the coordinates of the input image pixel to the point in the output image (or vice-versa)

$$x' = T_x(x,y) \qquad y' = T_y(x,y).$$

As mentioned previously, the geometric operations that are used the most in order to create a consistent forgeries are scaling, rotation, skewing, or any arbitrary combination. Hence, we focus our work on analyzing and detecting the traces of affine transformation. General affine transformation can be described by the following equations:

$$x' = a_0 + a_1 x + a_2 y \qquad y' = b_0 + b_1 x + b_2 y.$$

The second step in geometric transformations is called the interpolation step. Here, pixels intensity values of the transformed image are assigned using a constructed low-pass interpolation filter w. To compute signal values at arbitrary locations, as the word interpolation signifies[3] discrete samples of f_k are multiplied with the proper filter weights when convolving them with w.

Following the sampling theory, if the Nyquist criterion is satisfied, the spectrum $F(\omega)$ does not overlap in the Fourier domain. The original signal $f(x)$ can be reconstructed perfectly from its samples f_k using the optimal sinc interpolator. The sinc function is hard to implement in practice because of its infinite extent. Thus, many different simpler interpolation kernels of bounded support have been investigated and proposed so far [12]–[14]. We will be concerned mainly with following low-order piecewise local polynomials: nearest neighbor, linear, cubic, and truncated sinc. These polynomials are used extensively because of their simplicity and implementation unassuming properties.

Combining the derivative theorem with the convolution theorem leads to the conclusion that by convolution of f_k with a derivative kernel $\mathcal{D}^n\{w\}$, it is possible to reconstruct the nth derivative of $f(x)$. We denote the result of interpolation operation by $f^w(x)$, respectively, by $\mathcal{D}\{f^w\}(x)$. Formally

$$\begin{aligned} f^w(x) &= \sum_{k=-\infty}^{\infty} f_k w\left(\frac{x}{\Delta_x} - k\right) \\ \mathcal{D}^n\{f^w\}(x) &= \mathcal{D}^n\left\{\sum_{k=-\infty}^{\infty} f_k w\left(\frac{x}{\Delta_x} - k\right)\right\} \\ &= \sum_{k=-\infty}^{\infty} f_k \mathcal{D}^n\{w\}\left(\frac{x}{\Delta_x} - k\right). \end{aligned} \tag{2}$$

[3]The word "interpolation" originates from the Latin word "inter," meaning "between," and verb "polare," meaning "to polish" [1].

As pointed out in [15], it is easy to show that the covariance function of an interpolated image or its derivative is given by

$$\begin{aligned} R_{\mathcal{D}^n\{f^w\}}(x, x+\xi) = \sum_{k_1=-\infty}^{\infty}\sum_{k_2=-\infty}^{\infty} &\mathcal{D}^n\{w\}\left(\frac{x}{\Delta_x} - k_1\right) \\ &\times \mathcal{D}^n\{w\}\left(\frac{x+\xi}{\Delta_x} - k_2\right) R_f(k_1, k_2). \end{aligned}$$

If we assume the constant variance random process, then the variance of $\mathcal{D}^n\{f^w\}$, $\mathrm{var}\{\mathcal{D}^n\{f^w\}(x)\}$, as a function of the position x, can be represented in the following way:

$$\begin{aligned} \mathrm{var}\left\{\mathcal{D}^n\{f^w\}(x)\right\} &= R_{\mathcal{D}^n\{f^w\}}(x,x) \\ &= \sigma^2 \sum_{k=-\infty}^{\infty} \mathcal{D}^n\{w\}\left(\frac{x}{\Delta_x} - k\right)^2 \end{aligned} \tag{3}$$

where $\sigma^2 = R_n(k_1, k_2)$. This equation can be obtained if $R_f(k_1, k_2)$ has a short-range correlation [15]. Similarly, the covariance can be represented like

$$\begin{aligned} R_{\mathcal{D}^n\{f^w\}}(x, x+\xi) = \sigma^2 \sum_{k=-\infty}^{\infty} &\mathcal{D}^n\{w\}\left(\frac{x}{\Delta_x} - k\right) \\ &\times \mathcal{D}^n\{w\}\left(\frac{x+\xi}{\Delta_x} - k\right). \end{aligned}$$

Now, by assuming that ϑ is an integer, we can notice that

$$\mathrm{var}\left\{\mathcal{D}^n\{f^w\}(x)\right\} = \mathrm{var}\left\{\mathcal{D}^n\{f^w\}(x + \vartheta\Delta_x)\right\}, \vartheta \in \mathcal{Z}. \tag{4}$$

Thus, $\mathrm{var}\{\mathcal{D}^n\{f^w\}(x)\}$ is periodic over x with period Δ_x (as aforementioned, Δ_x is the sampling step). We verify this in the following way:

$$\begin{aligned} &\mathrm{var}\left\{\mathcal{D}^n\{f^w\}(x + \vartheta\Delta_x)\right\} \\ &\quad = \sigma^2 \sum_{k=-\infty}^{\infty} \mathcal{D}^n\{w\}\left(\frac{x + \vartheta\Delta_x}{\Delta_x} - k\right)^2 \\ &\quad = \sigma^2 \sum_{k=-\infty}^{\infty} \mathcal{D}^n\{w\}\left(\frac{x}{\Delta_x} - (k - \vartheta)\right)^2 \\ &\quad = \mathrm{var}\left\{\mathcal{D}^n\{f^w\}(x)\right\}. \end{aligned}$$

In other words, we have shown that interpolation brings into the signal and their derivatives a specific periodicity. This periodicity is dependent on the interpolation kernel used. Several widely used interpolation kernels will be studied in the next section.

Similarly, it can be shown that the covariance of f^w and $R_{\mathcal{D}^n\{f^w\}}(x, x+\xi)$ is periodic as well. The periodicity is apparent for offset $\xi = \vartheta\Delta_x, \vartheta \in \mathcal{Z}$

$$R_{\mathcal{D}^n\{f^w\}}(x, x+\xi) = R_{\mathcal{D}^n\{f^w\}}(x, x + \vartheta\Delta_x)\vartheta \in \mathcal{Z}.$$

Before going on, it can be interesting to have a look at the application of the Taylor series on $\mathcal{D}^n\{f^w\}(x)$. By application of the Taylor series, the hidden periodicity of the interpolation process can also be noticed and analyzed. By assuming that the

first $(m+1)$ derivatives of $f(x)$ exist, we can rewrite (2) as follows:

$$\mathcal{D}^n\{f^w\}(x) = \sum_{k=-\infty}^{\infty} \left\{ \sum_{m=0}^{m} \frac{\mathcal{D}^m\{f\}(x)}{m!}(k\Delta_x - x)^m + R_{m+1}(x, k\Delta_x)\right\} \mathcal{D}^n\{w\}\left(\frac{x}{\Delta_x} - k\right). \quad (5)$$

By defining

$$\tilde{T}_m(x) = \sum_{k=-\infty}^{\infty} \frac{(k\Delta_x - x)^m}{m!} \mathcal{D}^n\{w\}\left(\frac{x}{\Delta_x} - k\right)$$

and

$$\tilde{R}_{m+1}(x, k\Delta_x) = \sum_{k=-\infty}^{\infty} R_{m+1}(x, k\Delta_x)\mathcal{D}^n\left\{w\left(\frac{x}{\Delta_x} - k\right)\right\}$$

we can rewrite (5) as

$$\mathcal{D}^n\{f^w(x)\} = \sum_{m=0}^{m} \tilde{T}_m(x)\mathcal{D}^n\{f\}(x) + \tilde{R}_{m+1}(x, k\Delta_x).$$

Now, by analyzing $\tilde{T}_m(x)$, we can notice that it is periodic with period Δ_x as well

$$\begin{aligned}\tilde{T}_m(x + \vartheta\Delta_x) &= \sum_{k=-\infty}^{\infty} \frac{(k\Delta_x - (x + \vartheta\Delta_x))^m}{m!} \\ &\quad \cdot \mathcal{D}^n\{w\}\left(\frac{x + \vartheta\Delta_x}{\Delta_x} - k\right) \\ &= \sum_{k=-\infty}^{\infty} \frac{(\Delta_x(k - \vartheta) - x)^m}{m!} \quad \cdot \\ &\quad \cdot \mathcal{D}^n\{w\}\left(\frac{x}{\Delta_x} - (k - \vartheta)\right) \\ &= \tilde{T}_m(x)\end{aligned}$$

A. Multidimensional Extension

The theory studied in this section can be analogously extended for the multidimensional cases. If we assume that variance is one, $\vartheta \in \mathcal{Z}$ and operator $\mathcal{D}^n$ is a partial derivative, then (3) and (4) become

$$\operatorname{var}\{\mathcal{D}^n\{f^w\}(x, y)\} = \sum_{k=-\infty}^{\infty}\sum_{l=-\infty}^{\infty} \mathcal{D}^n\{w\}\left(\frac{x}{\Delta_x} - k, \frac{y}{\Delta_y} - l\right)^2 \quad (6)$$

$$\operatorname{var}\{\mathcal{D}^n\{f^w\}(x, y)\} = \operatorname{var}\{\mathcal{D}^n\{f^w\}(x + \vartheta\Delta_x, y + \vartheta\Delta_y)\}. \quad (7)$$

V. Resampled Signals

As it is apparent from (3), different interpolators change the structure of the signal in different ways. Fig. 2 shows the resulting periodic variance function computed via (3) with $\sigma = 1$ for the nearest neighbor interpolation. Nearest neighbor interpolator is a zero-degree kernel and the simplest of all piecewise, local polynomials. As it is shown, the variance is a constant function. Note that derivatives of the nearest neighbor polynomial are zero. Hence, signals interpolated by this interpolator can be easily recognized by applying a derivative operator to them.

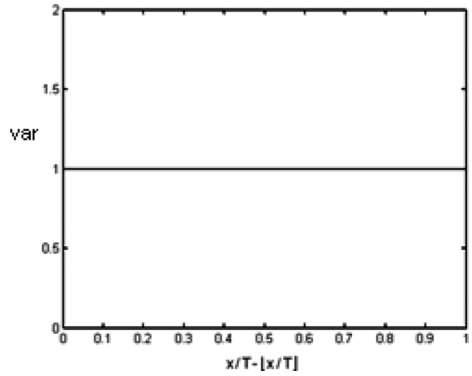

Fig. 2. Periodic variance function computed via (3) for the nearest-neighbor kernel.

Fig. 3 shows periodic variance functions generated via (3) with $\sigma = 1$ for linear interpolation, linear first, and linear second derivative kernels. The linear interpolation is a first-degree member of piecewise, local polynomials. It results in an interpolated signal which is continuous, but its first derivative is discontinuous.

In Fig. 4, the generated periodic variance functions (with $\sigma = 1$) for Catmull–Rom cubic interpolation and its first and second derivative interpolation kernels are illustrated. Cubic interpolation is a very frequently used interpolation technique and has been widely studied. It uses a third-order interpolation polynomial as the kernel.

In Fig. 5, the variance functions $(\sigma = 1)$ for truncated sinc (with six supporting points) interpolation, truncated sinc first, and second derivative interpolation kernels are shown.

VI. Detection of Periodic Properties of Resampled Images

In this section, we introduce a method capable of detecting the traces of resampling and interpolation using the periodic properties brought into the signal and its derivatives by low-order interpolation polynomials. The goal is to determine whether the signal being investigated or some of its portion has been resampled/interpolated or not. In concrete, we pay attention to individual transformations forming the affine transformation.

The proposed method is based on a few main steps: ROI selection, signal derivative computation, radon transformation, and search for periodicity. Each step is explained separately in the following sections.

A. Region of Interest Selection

In general, a typical image $f(x, y)$ consists of several consistent regions. To investigate whether any of these regions has been resampled, we select this region by a block of $R \times R$ pixels (we denote this block by $b(x, y)$) and apply the method to this image subset. If it is not possible to define any ROI in the given image or there is a need to find all resampled regions, the image can be tiled by overlapping blocks $b_i(x, y)$ of $R \times R$ pixels.

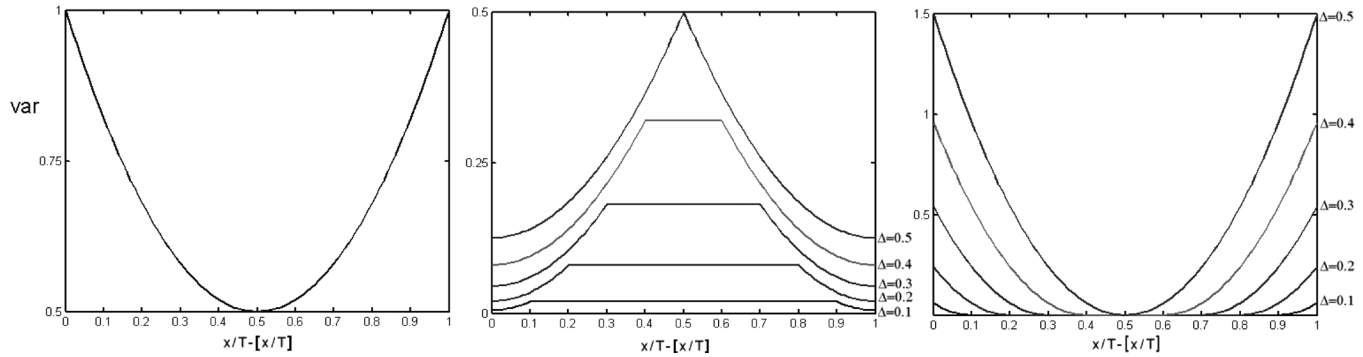

Fig. 3. Periodic variance of the linear, linear first, and second derivative kernel computed via (3).

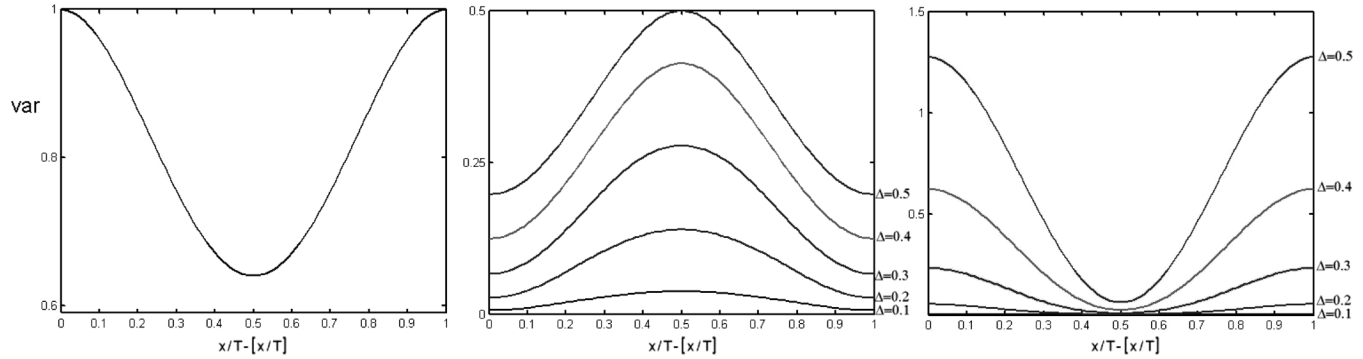

Fig. 4. Periodic variance of the cubic, cubic first, and second derivative kernel computed via (3).

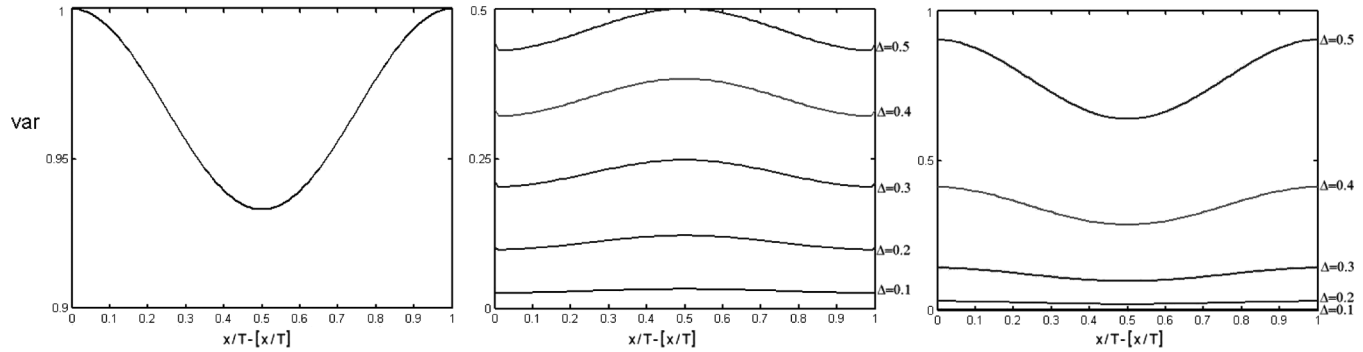

Fig. 5. Periodic variance of the truncated sinc, first, and second derivative truncated sinc kernel ($N = 6$).

Blocks can be horizontally slid by $N, N \in \mathcal{N}$ pixels rightwards starting with the upper left corner and ending with the bottom right corner. Each block can be analyzed by the method separately. In our experiments, R is mostly set to 128 pixels. In other words, we analyze windows of 128 $\times$ 128 pixels.

B. Signal Derivative Computation

To emphasize the presence of the periodic properties in the covariance structure of the resampled image, the nth derivative of the investigated region $b(x, y)$, $D^n\{b(x, y)\}$ is computed. This is accomplished by applying an approximate derivative operator calculating differences between adjacent pixels of rows of $b(x, y)$. In our experiments, the derivative order n is set to 2. The used derivative kernel is [1, −2, 1]. Similar results can be achieved by other derivative orders or using a laplace operator.

C. Radon Transformation

To be able to find traces of affine transformation, we employ a radon transformation. The radon transformation computes projections of magnitudes of $D^n\{b(x, y)\}$ along specified directions determined by angle θ (see Fig. 6). The projection is a line integral in a certain direction. The line integral can be expressed in the following way:

$$\rho_{D^n\{b\}}(x, y) = \int_L |D^n\{b(x, y)\}|\, dl.$$

By assuming that

$$\begin{bmatrix} x' \\ y' \end{bmatrix} = \begin{bmatrix} \cos\theta & \sin\theta \\ -\sin\theta & \cos\theta \end{bmatrix} \begin{bmatrix} x \\ y \end{bmatrix}$$

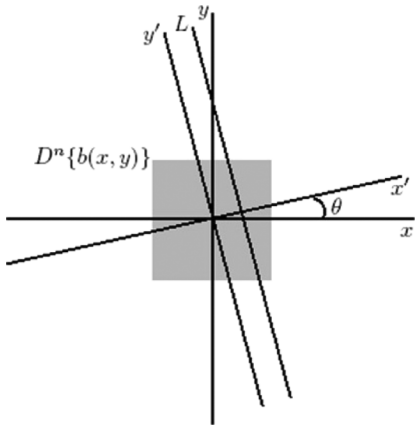

Fig. 6. Radon transformation.

it is possible to represent the radon transform in the following way:

$$\rho_\theta(x') = \int_{-\infty}^{\infty} |D^n\{b(x,y)\}| \cdot(x'\cos\theta - y'\sin\theta, x'\sin\theta + y'\cos\theta)dy'.$$

To compute the radon transformation, pixels are divided into four subpixels and each subpixel is projected separately. The radon transformation is computed at angles θ from 0 to 179°, in 1° increments. Hence, the output of this section is 180 1-D vectors, ρ_θ (θ denotes the orientation of the x' axis counterclockwise from the x axis, see Fig. 6).

D. Search for Periodicity

The previous section results in 180 vectors ρ_θ. If the investigated region has been resampled, the corresponding autocovariance sequences of ρ_θ contain a specific strong periodicity. The autocovariance can be computed in this way

$$R_{\rho_\theta}(k) = \sum_i (\rho_\theta(i+k) - \overline{\rho_\theta})\,(\rho_\theta(i) - \overline{\rho_\theta})\,.$$

As mentioned previously, our goal is only to determine if the image being investigated has undergone affine transformation. Hence, we focus only on the strongest periodic patterns present in the autocovariance sections R_{ρ_θ}. The effect of this could be that when the analyzed image has undergone several geometric transformations, our method may not detect all particular transformations present in this signal, but only those that have the clearest and strongest periodic properties.

To emphasize and easily detect the periodicity, a derivative filter of order one is applied to vectors ρ_θ. After this, in order to easily exhibit strong peaks signifying interpolation, the magnitudes of the fast Fourier transformation of obtained sequences R_{ρ_θ} are computed. To easily detect the mentioned periodicity, the magnitudes of FFT $|\mathrm{FFT}(R_{\rho_\theta})|$ are all combined and plotted together to create the main output of the method (for example, see Fig. 9). As will be apparent from the next section, if the analyzed region contains interpolation, peaks in the spectrum are very clear and strong and cannot be missed. The spectrum of such a signal has totally different properties of those noninterpolated signals (see Figs. 9 and 10). To automatically detect the interpolation peaks, we apply a simple and strict threshold-based peak detector searching for the local maximum (peaks n times greater than a local average magnitude).

It can be interesting to mention that the presented method can help to estimate the parameters of detected transformation. For example, in the case of rotation, peaks appearing in the spectrum can help us determine the angle of rotation transformation. Furthermore, as pointed out in [11], when we are concerned with scaling, there is a direct relation between the normalized position of interpolation peaks f_n and the scaling factor N

$$N = \begin{cases} \frac{1}{f_n}, & f_n \geq 0.5 \\ \frac{1}{1-f_n}, & f_n < 0.5. \end{cases}$$

The method described in this section is always separately applied also to the columns of $b(x,y)$. This is because of the fact that some transformations and images exhibit clearer periodicity in this direction.

So far, we were concerned with TIFF format images. When the method is applied to JPEG compressed images (we assume that the JPEG compression is carried out after the interpolation process), the processing of the method's output must be a little modified. As is well known, the JPEG compression technique divides the image into 8×8 pixel blocks to which DCT-based coding is applied. This blocking artifact brings into the image a periodicity producing peaks at normalized frequencies at positions 1/8, 2/8, 3/8, 5/8, 6/8, and 7/8 (this can be simply shown by applying the method to JPEG compressed images with a quality factor of 95 and lower). Therefore, when the output of the method is analyzed, these peaks should be ignored. Please note that peaks corresponding to a few resampling factors occur at the same positions as well. Hence, for these factors, it is not possible to make a decision using the presented method's output (for example, a scaling factor of 0.8 or 1.6, see Table I).

VII. Experimental Results

Fig. 7 shows a 2-D version of the described theory (7) for bilinear interpolation with scaling factor $N = 1.7$. The entries of the original 2-D signal have been chosen randomly from a normal distribution with mean zero and variance one. Fig. 8 illustrates that the theory studied in this paper works well for 1-D signals as well. Here, the theory has been applied to a 1-D cubic interpolated signal with interpolation factor $N = 0.9$. The results for both examples are shown for derivative operator D^n with $n = 0$ and 1.

Fig. 9 shows the output of the method applied to a resampled region of an investigated image (Fig. 1). The investigated image in this case consists of two parts, one of which is resized. It is apparent that peaks signifying resampling are strong and clearly detectable. Fig. 10 illustrates the case when this method is applied to a nonresampled region. It is apparent that the spectrum

TABLE I
DETECTION ACCURACY [%] AS A FUNCTION OF DIFFERENT SCALING FACTORS, TIFF, JPEG COMPRESSION QUALITIES, AND SIGNAL-TO-NOISE RATIOS. EACH CELL CORRESPONDS TO THE AVERAGE DETECTION ACCURACY FROM 40 IMAGES

scaling factor	0.55	0.60	0.65	0.70	0.75	0.80	0.85	0.90	0.95	0.97	0.99
TIFF	67	82	92	95	97	100	100	100	100	90	35
JPEG 100	67	82	92	95	97	0	100	100	100	90	35
JPEG 97	55	67	85	92	95	0	100	100	100	87	30
JPEG 95	42	55	70	77	85	0	87	90	85	57	12
SNR 50 dB	67	82	92	95	97	100	100	100	100	90	32
SNR 40 dB	60	80	90	92	97	100	100	100	100	87	25
SNR 30 dB	55	72	85	90	92	95	95	95	87	47	10
SNR 20 dB	5	5	7	10	10	10	12	12	5	5	0

scaling factor	1.01	1.03	1.05	1.10	1.15	1.20	1.25	1.30	1.35	1.40	1.45
TIFF	35	90	100	100	100	100	100	100	100	100	100
JPEG 100	35	90	100	100	100	100	100	100	100	100	100
JPEG 97	30	87	100	100	100	100	100	100	100	100	100
JPEG 95	12	57	87	95	95	100	100	100	100	100	100
SNR 50 dB	32	90	100	100	100	100	100	100	100	100	100
SNR 40 dB	25	87	100	100	100	100	100	100	100	100	100
SNR 30 dB	12	47	92	97	97	100	100	100	100	100	100
SNR 20 dB	0	7	7	12	15	17	20	20	25	27	30

scaling factor	1.50	1.55	1.60	1.65	1.70	1.75	1.80	1.85	1.95	2.05	2.10
TIFF	100	100	100	100	100	100	100	100	100	100	100
JPEG 100	100	100	0	100	100	100	100	100	100	100	100
JPEG 97	100	100	0	100	100	100	100	100	100	100	100
JPEG 95	100	100	0	100	100	100	100	100	100	100	100
SNR 50 dB	100	100	100	100	100	100	100	100	100	100	100
SNR 40 dB	100	100	100	100	100	100	100	100	100	100	100
SNR 30 dB	100	100	100	100	100	100	100	100	100	100	100
SNR 20 dB	30	30	30	30	30	30	30	30	30	30	30

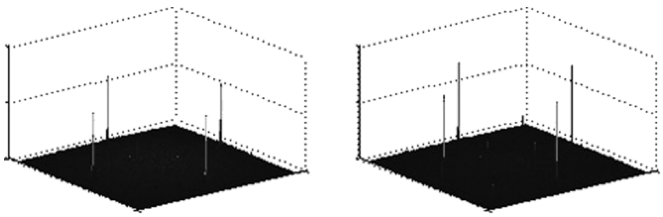

Fig. 7. Bilinear interpolation (interpolation factor 1.7).

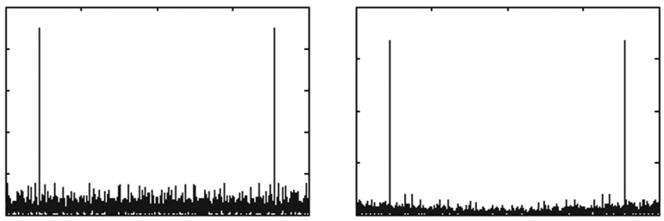

Fig. 8. Cubic interpolation (interpolation factor 0.9).

has totally different properties and there are no strong peaks signifying resampling. The size of the investigated window in both examples is 128 × 128 pixels.

Figs. 11–14 show outputs of the method applied to several TIFF format images that have undergone various transformations. The outcomes are shown based on rows derivative. The size of the investigated region (denoted by a black box) in all cases is 128 × 128 pixels. It is apparent that peaks signifying interpolation are clearly detectable. Fig. 15 shows the output of the method applied to a JPEG format interpolated image (with JPEG quality factor 95). The JPEG compression was carried out after the interpolation process. Here, despite the fact that peaks corresponding to JPEG have occurred, the resampling has been successfully recognized. Also here, the size of the investigated region is 128 × 128 pixels.

In the second part of this section, a quantitative measure of the efficiency of the proposed method is carried out. The method has been applied to 40 images corrupted by various transformations. For a few examples of the test images collection, see Fig. 16. The size of test images was 512 × 512 pixels. To perform a quantitative measure, the presented method has been applied to the whole image (in other words, the size of investigated region was 512 × 512 pixels). In all cases, the bicubic interpolation method was used. The method was applied separately to rows and columns of tested images. All experiments were carried out in Matlab.

Specifically, Table I shows the detection accuracy of the method applied to bicubic-resized images. The detection accuracy expresses the success of the method in expressing the interpolation by clear and easily detectable peaks, either in row-based or column-based output (for example, see Fig. 9). Note that the detection is nearly perfect for scaling factors greater than 1.03. Table II shows the detection accuracy of the proposed method applied to rotated images. Table III shows the detection accuracy of the proposed method applied to various skewing factors (skewing was applied to both x and y directions). The tables that are shown contain the detection accuracy of the method with respect to TIFF format images, lossy JPEG format for qualities 95, 97, 100, and white Gaussian noise with a signal-to-noise ratio (SNR) of 20, 30, 40, and 50. JPEG images were obtained from the noncompressed transformed images. Noisy images were obtained by adding white Gaussian noise to the noncompressed transformed images. First, the method has been applied to the rows of tested images. Then, the same was applied to the columns of tested images. For

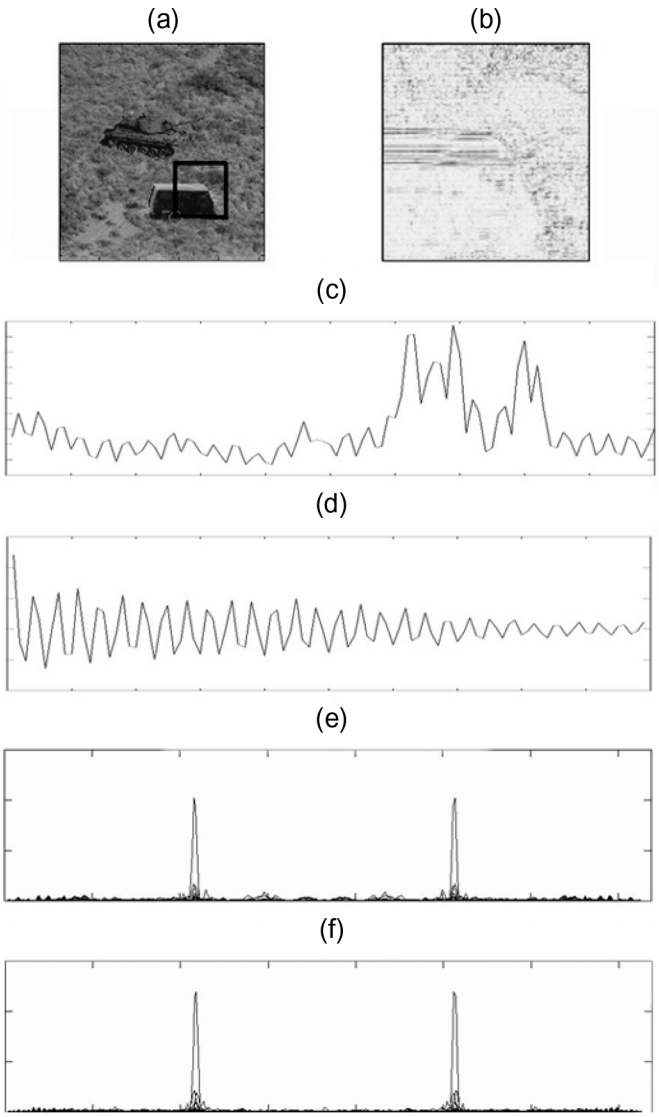

Fig. 9. Shown are: (a) the investigated region $b(x, y)$ (denoted by a black box, 128 × 128 pixels); (b) the magnitudes of the rows-based signal derivative $D^2\{b(x, y)\}$ (inverted); (c) the radon transformation output ρ_θ for $\theta = 90°$; (d) the autocovariance $R_{\rho_\theta}(\theta = 90°)$; (e) the row-based output of the proposed method ($|\mathrm{FFT}(R_{\rho_\theta})|$); and (f) the column-based output of the method. Peaks are clear and signify interpolation. The radon transformation was computed at angles θ from 0 to 179°, in 1° increments. The investigated image is shown in Fig. 1.

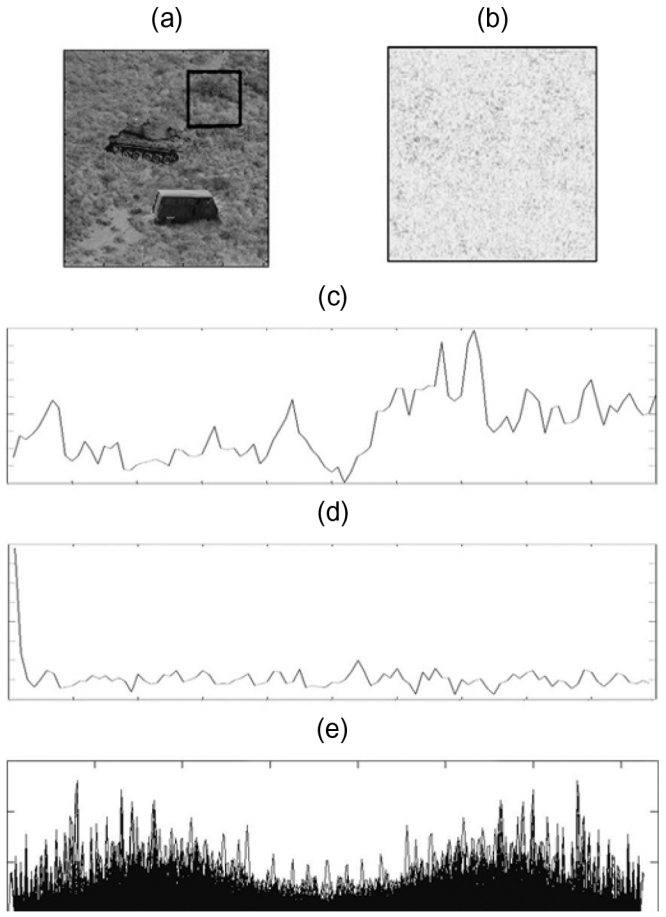

Fig. 10. Shown are: (a) the investigated region $b(x, y)$ (denoted by a black box, 128 × 128 pixels); (b) the magnitudes of the row-based signal derivative $D^2\{b(x, y)\}$ (inverted); (c) the radon transformation output ρ_θ for $\theta = 90°$; (d) the autocovariance $R_{\rho_\theta}(\theta = 90°)$; (e) the row-based output of the proposed method ($|\mathrm{FFT}(R_{\rho_\theta})|$). The radon transformation was computed at angles θ from 0 to 179° in 1° increments. The investigated region has not undergone any geometric transformation. Hence, there are no clear or strong peaks. The spectrum has totally different properties compared to Fig. 9. The investigated image is shown in Fig. 1.

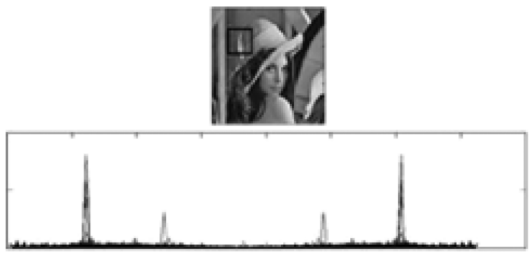

Fig. 11. Scaling factor = 1.2 (nearest-neighbor interpolation). The investigated region is denoted by the black box.

correctly detected resized TIFF format images, we also tried to estimate the particular scaling factors using the position of the occurring interpolation peaks. This was carried out for scaling factors greater than 1.03 shown in Table I. The estimation process was based on finding the global maximum in the output of the method. The detection accuracy was close to 100%. The same was carried out for rotated TIFF format images (for rotation angles greater than 3° shown in Table II). Also here, based on the interpolation peaks positions, we tried to estimate the particular rotation angles. The detection accuracy was again near 100%.

During the experimental phase, the method was also applied to the original (noninterpolated) versions of tested images. This resulted in a false positive rate of 12%. Most of the false positives were caused by strong textures or strong color filter array (CFA) interpolation in some of the test images. Since the method is focused on searching for periodic traces of interpolation, non-interpolated images containing often strong periodicities can yield an output similar to interpolated images. This limitation probably will occur in all methods concerned with the periodic patterns of interpolation. In our method, we prefer to have a higher false positive rate than missing forgery. To strengthen our evidence of forgery, other existing forgery detection methods as well as a texture and CFA analyzing step can be employed.

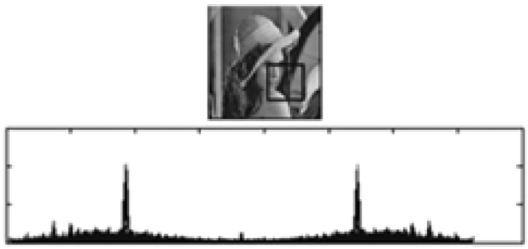

Fig. 12. Scaling factor = 0.8 (bicubic interpolation).

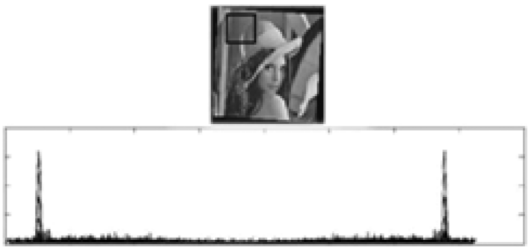

Fig. 13. Rotation = -4° (bilinear interpolation).

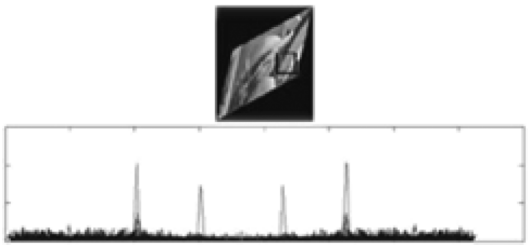

Fig. 14. Skewing factor in x direction = -0.4, in y direction = -0.4 (bilinear interpolation); rotation = 10° (bilinear interpolation).

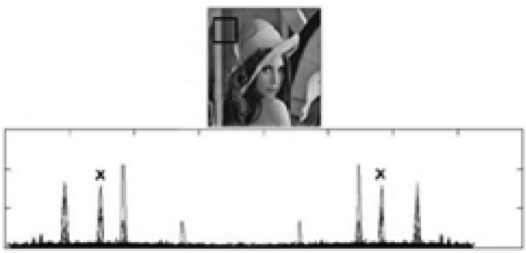

Fig. 15. Scaling factor = 1.25 (bicubic interpolation). JPEG format with quality factor 95. Peaks corresponding to the scaling transformation are denoted by $\times$. Other peaks belong to JPEG blocking artifacts.

Fig. 16. Few examples of test images.

TABLE II
DETECTION ACCURACY [%] AS A FUNCTION OF DIFFERENT ROTATION ANGLES, TIFF, JPEG COMPRESSION QUALITIES, AND SNRS. EACH CELL CORRESPONDS TO THE AVERAGE DETECTION ACCURACY FROM 40 IMAGES

rotation angle	1°	3°	5°	10°	15°	20°	30°	40°
TIFF	22	85	100	100	100	100	100	100
JPEG 100	22	85	100	100	100	100	100	100
JPEG 97	17	77	100	100	100	100	97	92
JPEG 95	7	57	92	100	100	97	85	70
SNR 50 dB	22	85	100	100	100	100	100	100
SNR 40 dB	17	80	100	100	100	100	100	100
SNR 30 dB	10	52	90	100	100	100	87	90
SNR 20 dB	0	5	12	20	22	25	12	10

VIII. DISCUSSION

Obtained results show that the proposed method makes it possible in a simple and fast way to find traces of general affine transformation when a low-order interpolation polynomial has been used.

Please note that not all resampling operations bring detectable changes into the covariance structure of the signal. For instance, the scaling factor 0.5 does not introduce any periodic correlation. This can be easily noticed from its resampling matrix (by the resampling matrix, we understand the matrix $\mathbf{M}$, where $f^r = \mathbf{M}f_k$)

$$\mathbf{M_{0.5}} = \begin{pmatrix} 1 & 0 & 0 & 0 & 0 & \\ 0 & 0 & 1 & 0 & 0 & \\ 0 & 0 & 0 & 0 & 1 & \\ & & & & & \ddots \end{pmatrix}.$$

Furthermore, it must be noted that because of aliasing, there are resampling factors which have indistinguishable periodic patterns (for example, scaling factors 1.5 and 3). For these factors, peaks in the spectrum occur in the same positions. This can be noticed also by analyzing the resampling matrix of these interpolation factors. Hence, the presented method itself cannot propose uniqueness in the estimaton of resampling factors.

The proposed method works well for low-order interpolation polynomials: nearest neighbor, linear, or cubic. These interpolators have a strong detectable effect on the covariance structure of the signal. The detection performance decreases as the order of interpolation polynomial increases. Different interpolation orders introduce correlations of varying degrees between neighboring samples. These correlations become more difficult to detect as each interpolated sample value is obtained as a function of more samples. For example, in an image interpolated by a truncated sinc with $N = 9$, interpolated pixels are functions of 81 pixels. Note that when the ideal sinc interpolator is used, the covariance structure of the signal does not change and, therefore, this interpolator is not detectable. This statement can be shown by evaluating (3) for sinc, which gives 1 for all x (it is due to the fact that $\sum_{k=-\infty}^{\infty} \mathcal{D}^n\{\mathrm{sinc}\}(x-k)^2 = 1$).

It must be mentioned that the results obtained can be affected by the presence of other correlations in the signal. Hence, the best results are obtained by applying the method to an interpolated white noise signal (the autocorrelation of a white noise signal has a strong peak at $x = 0$ and is close to 0 elsewhere).

The proposed method is based on a statistical approach. It could be said that larger investigated regions give stronger and

TABLE III
DETECTION ACCURACY [%] AS A FUNCTION OF DIFFERENT SKEWING FACTORS, TIFF, AND SNR 40 dB. EACH CELL CORRESPONDS TO THE AVERAGE DETECTION ACCURACY FROM 40 IMAGES

skewing factor	0.01	0.03	0.05	0.10	0.15	0.20	0.25	0.30	0.35	0.40
TIFF	5	90	97	100	100	100	100	100	100	100
SNR 40 dB	0	0	0	0	0	0	0	0	0	0

more accurate results. Our experiments show that generally the smallest acceptable size of investigated regions is 128×128 pixels. But we have to mention that, for instance, many resampling operations can be recognized in a smaller investigation window (64×64 pixels) as well. On the other hand, some strong skewing factors need a larger investigation window. It depends on the signal spatial correlation and distribution of image pixels.

By applying the method to JPEG-compressed images (when JPEG compression is carried out after the interpolation process), the detection performance decreases. JPEG is a lossy compression format. It brings noise into the image. Experiments show that the presented method works well for JPEG compression quality of 95–100. But generally, the results obtained are based on image properties. By adding noise to the signal, the interpolation-based pixels correlation becomes corrupted and difficult to detect.

In this work, we were concerned with gray-level images. There are several ways to use the presented method for RGB images. For instance, the method can be applied to each channel separately.

IX. CONCLUSION

In this paper, we have analyzed specific periodic properties present in the covariance structure of interpolated signals and their derivatives. Furthermore, we have introduced a brief 2-D extension of the described theory. Also, we have analyzed an application of Taylor series to the interpolated signals. The main contribution of the paper is a method capable of easily detecting traces of scaling, rotation, skewing transformations, and any of their arbitrary combinations. The method is fast, blind, and efficient. It works for a wide variety of resampling factors. Another advantage of the method is that it can be very helpful in the estimation of scaling factors or rotation angles.

We believe that the theory studied here can be useful in image security and authentication as well as in applications based on statistical approaches using interpolated signals.

REFERENCES

[1] E. Meijering, "A chronology of interpolation: From ancient astronomy to modern signal and image processing," *Proc. IEEE*, vol. 90, no. 3, pp. 319–342, Mar. 2002.
[2] M. M. Yeung, "Digital watermarking," *Commun. ACM*, vol. 41, no. 7, pp. 30–33, 1998.
[3] C. Rey and J.-L. Dugelay, "A survey of watermarking algorithms for image authentication," *EURASIP J. Appl. Signal Process. Special Issue Image Anal. Multimedia Interactive Services*, vol. 2002 N6, pp. 613–621, Jun. 2002.
[4] J. Fridrich, "Methods for tamper detection in digital images," in *Proc. Multimedia Security Workshop at ACM Multimedia*, pp. 19–23.
[5] B. Mahdian and S. Saic, "Detection of copy-move forgery using a method based on blur moment invariants," *Forens. Sci. Int.*, vol. 171, no. 2–3, pp. 180–189, 2007.
[6] J. Fridrich, D. Soukal, and J. Lukas, "Detection of copy-move forgery in digital images," in *Proc. Digital Forensic Research Workshop*, Cleveland, OH, Aug. 2003, pp. 55–61, IEEE Comput. Soc.
[7] A. C. Popescu and H. Farid, "Exposing digital forgeries by detecting traces of re-sampling," *IEEE Trans. Signal Process.*, vol. 53, no. 2, pp. 758–767, Feb. 2005.
[8] M. K. Johnson and H. Farid, "Exposing digital forgeries by detecting inconsistencies in lighting," in *Proc. ACM Multimedia and Security Workshop*, New York, 2005, pp. 1–9.
[9] A. C. Popescu and H. Farid, "Statistical tools for digital forensics," in *Proc. 6th Int. Workshop Information Hiding*, Toronto, ON, Canada, 2004, pp. 128–147.
[10] S. Prasad and K. R. Ramakrishnan, "On resampling detection and its application to image tampering," in *Proc. IEEE Int. Conf. Multimedia Expo.*, Toronto, ON, Canada, 2006, pp. 1325–1328.
[11] A. C. Gallagher, "Detection of linear and cubic interpolation in JPEG compressed images," in *Proc. 2nd Canadian Conf. Computer Robot Vision*, Washington, DC, 2005, pp. 65–72, IEEE Comput. Soc.
[12] J. A. Parker, R. V. Kenyon, and D. E. Troxel, "Comparison of interpolation methods for image resampling," *IEEE Trans. Med. Imag.*, vol. MI-2, no. 1, pp. 31–39, Mar. 1983.
[13] H. Hou and H. Andrews, "Cubic splines for image interpolation and digital filtering," *IEEE Trans. Acoust., Speech Signal Process.*, vol. ASSP-26, no. 6, pp. 508–517, Dec. 1978.
[14] E. H. W. Meijering, W. J. Niessen, and M. A. Viergever, "Piecewise polynomial kernels for image interpolation: A generalization of cubic convolution," in *Proc. Int. Conf. Image Processing*, 1999, pp. 647–651.
[15] G. K. Rohde, C. A. Berenstein, and D. M. Healy, "Measuring image similarity in the presence of noise," in *Proc. SPIE Medical Imaging: Image Processing*, Feb. 2005, vol. 5747, pp. 132–143.

Babak Mahdian received the M.Sc. degree in computer science from the University of West Bohemia, Pilsen, Czech Republic, in 2004, and the Ph.D. degree in mathematical engineering from the Czech Technical University, Prague, Czech Republic, in 2008.

Currently, he is with the Institute of Information Theory and Automation, Academy of Sciences of the Czech Republic, Prague. His current research interests include all aspects of digital image processing and pattern recognition, particularly digital image forensics, interpolation theory, facial expressions recognition, and multimodal HCI.

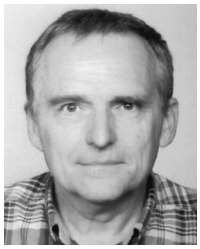

Stanislav Saic received the M.Sc. degree in physical electronics from the Czech Technical University, Prague, Czech Republic, in 1973, and the C.Sc. degree (corresponding to the Ph.D. degree) in radio electronics from the Czechoslovak Academy of Sciences, Prague, in 1980.

Since 1973, he has been with the Institute of Information Theory and Automation, Academy of Sciences of the Czech Republic, Prague, where he was Head of the Department of Image Processing from 1985 to 1994. His current research interests include all aspects of digital image and signal processing, particularly Fourier transform, image filters, remote sensing, and geosciences.